Desalination and Water Treatment
www.deswater.com
doi: 10.5004/dwt.2021.27181

224 (2021) 95–105
June

Preparation and anti-fouling performance of polyvinylidene fluoride composite membranes modified with different contents of TiO_2/GO

Huiya Wang[a,*], Keqiang Ding[a], Qiang Zhou[b]

[a]*School of Environmental Engineering, Nanjing Institute of Technology, No. 1 Hongjing Avenu Jiangning Science Park, Nanjing, Jiangsu, PR. China, CN211167, emails: wlyplgl@njit.edu.cn (H. Wang), dingkq@njit.edu.cn (K. Ding)*
[b]*Jiangsu Peier Membrane Industry Co. Ltd., Yixing, Jiangsu, PR. China, CN214200, email: peier@pe314.com*

Received 24 September 2020; Accepted 18 February 2021

ABSTRACT

In this study, we report a new method for the *in situ* preparation of a polyvinylidene fluoride (PVDF)-based composite membrane. The strategy used in this method involves the combination of a one-step synthesis of the gel–sol method with a traditional immersion precipitation process. The TiO_2/GO (graphene oxide) composite was uniformly dispersed in N,N-dimethylformamide solution in different proportions, and then the PVDF polymer was dissolved into the resulting N,N-dimethylformamide sol system to obtain a homogeneous casting solution. A homogeneous TiO_2/GO/PVDF casting solution was then obtained by dissolving PVDF in the N,N-dimethylformamide (DMF) sol with different contents of TiO_2/GO particles. Scanning electron microscopy (SEM), X-ray diffraction, and X-ray photoelectron spectroscopy analysis showed that the prepared composite particles were a uniform mixture of TiO_2 and GO. Based on the precipitation kinetics and membrane morphology, we proved that the introduction of TiO_2/GO particles accelerated the phase inversion of the casting solution and made the pore diameter and pore diameter of the composite membrane change. The performance test of the composite membrane showed that TiO_2/GO and PVDF were effectively bonded, TiO_2/GO was transferred to the membrane surface during the phase conversion process, and the hydrophilicity of the composite membrane surface was enhanced. From the results of the separation and anti-fouling properties of the composite membrane, the composite membrane with 5% TiO_2/GO particles had excellent anti-fouling properties.

Keywords: Gel–sol method; Different content; Uniform mixture; Phase conversion; Bovine serum albumin

1. Introduction

Among the many water treatment technologies available, membrane separation has been extensively used to remove pollutants from wastewater due to the low energy consumption, high separation efficiency, and environmentally friendly characteristics [1,2]. Polyvinylidene fluoride (PVDF) is a type of polymer material widely used in the production of ultrafiltration membranes. PVDF has good mechanical properties, thermal stability, and chemical stability and is very popular in the water treatment industry. However, the hydrophobic nature of PVDF membranes makes it easy to adsorb or accumulate organic matter on the surface and inside [3], resulting in membrane pollution, resulting in a rapid decrease of water flux, and directly affecting the work efficiency and service life. Therefore, researchers around the world have performed extensive and in-depth studies on how to improve the anti-fouling performance of membrane materials [4–6].

When γ-Al_2O_3, ZrO_2, SiO_2, TiO_2, FeOOH, Al_2O_3, Fe_3O_4, and other inorganic nanoparticles [7–18] were added to the casting liquid system, the hydrophilic separation and

* Corresponding author.

pollution resistance of the prepared PVDF composite membranes were greatly improved. Many studies verified that the antibacterial and antifouling properties of porous polymer membranes can be significantly improved by modification with nanoparticles, such as TiO_2 [19–24]. Bet-Moushoul et al. [25] prepared a TiO_2/PVDF hybrid membrane by blending TiO_2 nanoparticles with PVDF. The results showed that the surface of TiO_2 particles is rich in hydroxyl groups, which can effectively improve the hydrophilicity of the membrane and improve the mechanical properties and anti-fouling effects of the hybrid membrane.

In recent years, the coupling of photocatalytic technology and membrane separation technology of TiO_2 has attracted the attention of scientists for new membrane materials [26–30]. However, in practical applications, TiO_2 is difficult to recover, easy to agglomerate in membrane systems, and has a low photocatalytic efficiency. In membrane separation technology, it has become a research hotspot to modify TiO_2 to improve its efficiency, and then to integrate it with an ultrafiltration membrane to better stimulate the synergistic effect of the two [31–35]. Graphene oxide (GO) has recently attracted great interest due to its large specific surface area, good water-dispersion ability, and high adsorption capacity [36–38]. Additionally, GO sheets can be a proper host for the decoration and dispersion of other inorganic nanoparticles, which makes it more appropriate for the modification of polymeric membranes [39–41]. Adding GO particles to TiO_2 nanosheets may allow us to efficiently impart antibacterial, antifouling, and selectivity characteristics to the sheets [42].

Safarpour et al. [43] dispersed TiO_2 in a PVDF casting solution after modification by GO, and the hybrid membrane demonstrated excellent photocatalytic performance. The hydrophilicity, degradation rate, and anti-fouling of the membrane were significantly improved. Shao et al. [44] and others analyzed and compared the introduction of TiO_2, GO, and TiO_2/GO into the membrane matrix, and found that the TiO_2/GO particles had a more distinct effect on improving the hydrophilicity and separation of the membrane.

Ayyaru et al. [45] used GO with TiO_2, and TiO_2/GO composite particles prepared by the sol-gel method. The influence of the introduction of composite particles on the structure and properties of ultrafiltration membranes was explored. Through a series of characterizations, the morphology and properties of the composite membranes changed greatly. Compared with pure membranes, the roughness of the composite membranes increased, the hydrophilicity increased, the contact angle decreased, and the water flux increased. The retention and photocatalysis were all improved.

In this study, TiO_2/GO composite particles were prepared with a one-step synthesis method on the existing basis. Scanning electron microscopy (SEM), X-ray diffraction (XRD), and X-ray photoelectron spectroscopy (XPS), and Fourier-transform infrared spectroscopy (FTIR) were used to analyze the microparticles. Then, we added different contents of TiO_2/GO to the PVDF casting solution. Based on the phase transformation mechanism, a simple casting method was used to prepare TiO_2/GO/PVDF composite membranes. The effect of different TiO_2/GO contents on the properties of membranes was investigated based on the pure water flux, static water contact angle, FTIR, surface and cross-section morphology, and fouling tests. The separation performance of the prepared membranes was studied by the rejection of bovine serum albumin (BSA). The anti-fouling performance of the membranes was evaluated by the recovery rate of the water flux and the time extended for flux attenuation of 30%.

2. Experimental

2.1. Reagents and instruments

We used titanium tetraisopropoxide (TIPO, Sigma-Aldrich, Germany); triethanolamine (TEOA, Xilong Chemical Co., Ltd., China); graphene oxide (GO, Sinopharm Chemical Reagent Co., Ltd., China); polyvinylidene fluoride (PVDF, Shanghai San Ai Fu New Material Co., Ltd., China); N,N-dimethylformamide (DMF, Sinopharm Chemical Reagent Co., Ltd., China); polyethylene glycol PEG6000 (Sinopharm Chemical Reagent Co., Ltd., China); and bovine serum albumin (BSA, formula weight 67000, Sinopharm Chemical Reagent Co., Ltd., China). The morphology and structure of the samples were characterized by transmission electron microscopy (JEM-200CX) and scanning electron microscopy (SEM, HITACHI S-3400N II, Japan). Powder X-ray diffraction (XRD) patterns were recorded on a Bruker D8 Multipurpose XRD system (Germany). FTIR spectroscopy was performed on a Nicolet iS10 spectrometer (United States). XPS and valence band X-ray photoelectron spectroscopy spectra were performed on a PHI 5000 VersaProbe instrument (China) with binding energies referenced to adventitious carbon at 284.6 eV.

2.2. Preparation of TiO_2/GO composites

We mixed 36.62 g of titanium tetraisopropanol and 38.06 g of triethanolamine, and added the mixture into a 250 mL volumetric flask for calibration with ultrapure water. We injected nitrogen into the volumetric flask for 3 min, sealed the mouth with sealing tape, and then used it as the mother liquor (including 10.3 g TiO_2). We measured 40 mL of ultra-pure water and added 0.515 g of graphene oxide. After ultrasonic treatment at 400 W power for 2 h, the graphene oxide was uniformly dispersed in the aqueous solution. We measured 40 mL of the mother liquor and ultra-pure water dispersed with graphene oxide and added them to the hydrothermal reactor with a polytetrafluoroethylene lining. We slowly added high-concentration sodium hydroxide solution to the reactor until the pH was 12 and kept it at 190°C for 24 h. Finally, we washed and filtered the product, put it into a muffle furnace, calcined it at 400°C for 2 h, and obtained the final TiO_2/GO composites [45].

2.3. Preparation of the TiO_2/GO/PVDF composite membrane

The TiO_2/GO composite was uniformly dispersed in N,N-dimethylformamide solution in different proportions, and then the PVDF polymer was dissolved into the resulting DMF sol system to obtain a homogeneous casting solution. A homogeneous TiO_2/GO/PVDF casting solution was then

obtained by dissolving PVDF in the DMF sol with different content TiO_2/GO particles. Specifically, we weighed 2.7 g of PEG6000 and dissolved it in 90 mL of DMF. We slowly added 12 g of PVDF, raised the temperature to 60°C, and mixed with the magnetic force for 4 h until it was completely dissolved. We added a certain proportion of TiO_2/GO composites in batches and continued to mix with the magnetic force for about 2 h to obtain a transparent and uniform TiO_2/GO/PVDF membrane casting solution.

After the prepared casting solution of the membrane was standing and defoaming at room temperature for 12 h, we poured the solution on the flat membrane equipment at 25°C and scraped to form a homogeneous membrane with an average thickness of 0.2 mm. After standing in the air for approximately 30 s, we immersed it in the coagulation bath (deionized water) at room temperature to form the membrane. We left the membrane standing in deionized water for 24 h for standby. In this study, PVDF composite membranes with different content of TiO_2/GO (1%, 3%, 5%, and 7%) were prepared and named PVDF-1, PVDF-2, PVDF-3, and PVDF-4. A pure PVDF membrane was prepared by the same method and named PVDF-0. The detailed preparation process was shown in Fig. 1.

2.4. TiO_2/GO composites characterization

SEM analysis was completed using a JSM-6380LV scanning electron microscope from Japan's JEOL Company. FTIR analysis was completed using a Tensor 27 Fourier-infrared spectrometer of Germany's Bruker Company. XRD analysis was completed using a D8 ADVANCE X-ray diffractometer of Germany's Bruker Company; X-ray photoelectron spectra were recorded on a Thermo Escalab 250Xi X-ray photoelectron spectrometer (XPS).

2.5. Characterization of the TiO_2/GO/PVDF composite membrane

SEM analysis using JSM-6380LV from Japan's JEOL Company was completed with a voltage of 30 kV. FTIR analysis was completed using a Tensor 27 Fourier-infrared spectrometer from Germany's Bruker Company. XRD was performed using a D8 ADVANCE X-ray diffractometer from the Bruker Company in Germany. Thermogravimetric analysis was performed using a SDT Q600 from the TA Company in the United States.

2.6. Ultrafiltration performance of TiO_2/GO/PVDF hybrid membrane

A self-made ultrafiltration device was used to test the water flux of the hybrid membrane, and the appropriate size of the membrane (50 cm^{-2}) was cut (Fig. 2). Under the pressure of N_2, the membrane was pre-compressed for 30 min under a pressure of 0.15 MPa. After adjusting the pressure to 0.1 MPa, the pure water flux (J_w, L m^{-2} h^{-1}) of the membrane was measured. Then, the deionized water was changed into 1 g of BSA solution, and the above operations were repeated to determine the membrane flux (J_p, L m^{-2} h^{-1}) of the hybrid membrane to the pollutant solution. Simultaneously, the UV-2100 UV-Vis spectrophotometer from Unocal Shanghai Instrument Co., Ltd., (China) was used to measure the BSA retention at 280 nm (the wavelength of BSA is 280 nm). The porosity was measured using the dry wet membrane method. All the above data were measured five times, and the average value was taken.

The specific formulas are as follows:

$$J_w = \frac{V_w}{A \times t} \tag{1}$$

$$J_p = \frac{V_p}{A \times t} \tag{2}$$

$$R = \left(1 - \frac{C_1}{C_0}\right) \times 100\% \tag{3}$$

$$\varepsilon = \frac{m_{\text{wet}} - m_{\text{dry}}}{m_{\text{wet}}} \times 100\% \tag{4}$$

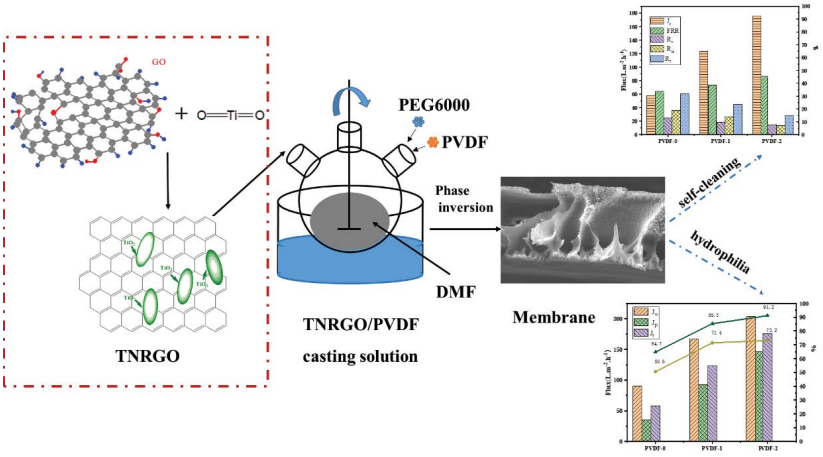

Fig. 1. The preparation flow chart of the composite membrane. Polyethylene glycol PEG6000, N,N-dimethylformamide, and polyvinylidene fluoride.

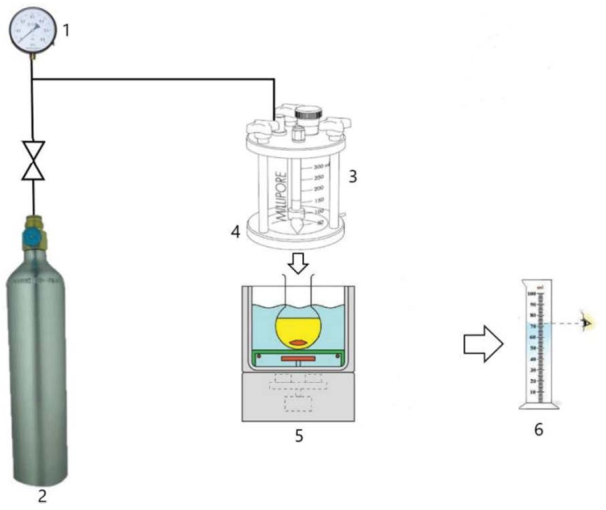

Fig. 2. Ultrafiltration device. (1) Pressure gauge; (2) nitrogen pressure cylinder; (3) ultrafiltration cup; (4) membrane test; (5) magnetic stirrers; (6) measuring cylinder.

where V_w (L) is the volume of pure water passing through the membrane, V_p (L) is the volume passing through the bovine serum albumin solution, A (m^2) is the area of the tested membrane, t (h) is the test time, C_0 (g/L) is the initial concentration of the bovine serum albumin solution, C_1 is the concentration of the bovine serum albumin solution in the filtrate, m_{wet} is the mass completely soaked in deionized water, and m_{dry} is the mass at the constant weight in the oven at 60°C.

The mean pore radius r_m of the membrane was determined using the filtration velocity method and was calculated from the Guerout–Elford–Ferry equation [46]:

$$r_m = \sqrt{\frac{(2.9 - 1.75\varepsilon) \times 8\eta l Q}{\varepsilon \times A \times \Delta P}} \quad (5)$$

where η denotes the water viscosity (8.9×10^{-4} Pa s), ε signifies the membrane porosity (%), l is the membrane thickness (m), Q is the volume of permeating water per unit time ($m^3\ s^{-1}$), A is the membrane active area (m^{-2}), and ΔP is the operation pressure (0.1 MPa).

2.6.1. Hydrophilicity

The dynamic contact angle of the film was measured using the drop method. The contact angle of the membrane was completed using the Hebei Chengde Dingsheng Co., Ltd., (China) testing equipment JY-82C. The phase separation rate of the casting solution was completed using a UV-2100 UV-visible spectrophotometer from the Unocal Shanghai Instrument Co., Ltd., (China) and the bottom 10 mm part of two cuvettes were wrapped with black tape to avoid UV penetration. We placed 2 mL of deionized water into a cuvette as a blank. We added 1 mL of casting solution to another quartz cuvette, placed the cuvette into the UV spectrophotometer, took 1 mL of deionized water, dropped it into the cuvette, and quickly closed the UV spectrophotometer. We set the UV spectrophotometer to record the absorbance value of DMF at 257 nm every 4 s for 10 min.

2.6.2. Pollution resistance

The membrane used in 2.6.1 was rinsed repeatedly with deionized water, and then the pure water (J_r, $L\ m^{-2}\ h^{-1}$) was tested again with deionized water. The recovery rate of the membrane flux (FRR, %), total pollution rate (R_{FD}, %), reversible pollution rate (R_r, %), and irreversible pollution rate (R_{ir}, %) were determined using specific calculation formulas as follows [47]:

$$\mathrm{FRR} = \frac{J_r}{J_w} \times 100\% \quad (6)$$

$$R_{\mathrm{FD}} = \frac{J_w - J_p}{J_w} \times 100\% \quad (7)$$

$$R_i = \frac{J_r - J_p}{J_w} \times 100\% \quad (8)$$

$$R_{\mathrm{ir}} = R_{\mathrm{FD}} - R_i \quad (9)$$

3. Results and discussion

3.1. TiO_2/GO composite

The morphology of the prepared TiO_2/GO composite was observed using SEM. As shown in Figs. 3a and b, the TiO_2/GO composite essentially maintained the morphology of TiO_2, which may be due to the small amount of GO. In addition, the element composition of the complex was further analyzed with energy-dispersive X-ray spectroscopy. From Fig. 3c, it can be clearly seen that the composite is composed of C, O, and Ti elements, in which the Ti element came from the prepared TiO_2, the O element came from TiO_2 and graphite oxide, and the C element came from graphene oxide, which further explains the successful combination of GO and TiO_2.

An X-ray diffractometer was used to study the crystal structure of the TiO_2/GO composite. As shown in Fig. 4, there are characteristic peaks at 11.1° and 42.6° in the XRD spectrum of GO, corresponding to the (002) crystal surface of GO. There are obvious diffraction peaks at 25.6°, 38.1°, 48.2°, 54.1°, 55.2°, 62.9°, 69.1°, 70.6°, and 75.4° in the XRD spectrum of TiO_2, which shows that the TiO_2 we synthesized was anatase crystal type [48]. The TiO_2/GO composite shows the characteristic peak of TiO_2, and there are weak diffraction peaks at 27.2°, 36.2°, and 37.2° in the XRD spectrum of TiO_2/GO, which may be caused by the synergistic effect of TiO_2 and GO. However, no characteristic peak of GO was observed, which may be due to the low content of GO in the composite or the relatively uniform distribution of GO on the TiO_2 surface.

XPS data provided more information on the surface composition and binding interactions of TiO_2/GO compounds. The Ti 2p region (Fig. 5a) depicts three peaks at 458.6, 461.3, and 464.4 eV. The peaks appearing at 458.6

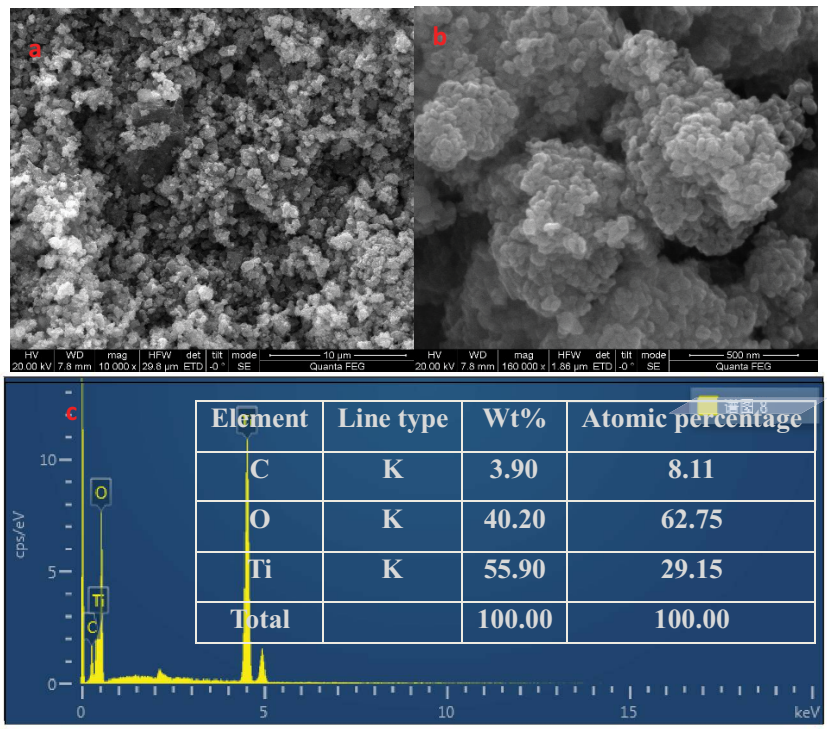

Element	Line type	Wt%	Atomic percentage
C	K	3.90	8.11
O	K	40.20	62.75
Ti	K	55.90	29.15
Total		100.00	100.00

Fig. 3. Scanning electron microscopy (SEM) of (a) TiO_2, (b) TiO_2/GO, and (c) element distribution.

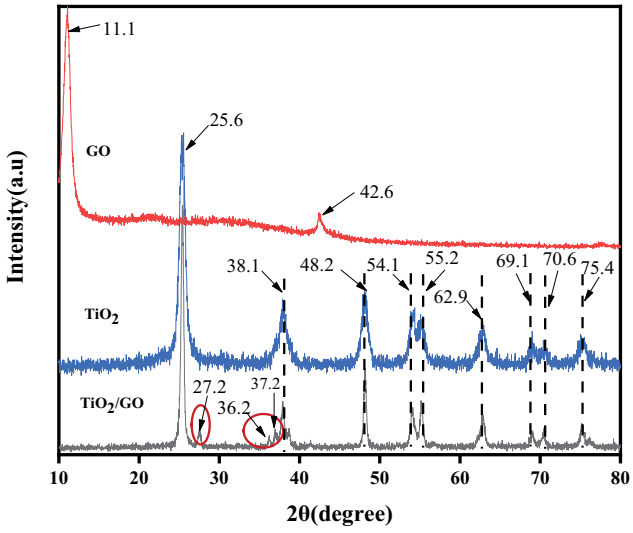

Fig. 4. X-ray diffraction (XRD) of GO, TiO_2, and TiO_2/GO.

and 464.4 eV can be assigned to Ti $2p_{3/2}$ and Ti $2p_{1/2}$ of TiO_2, verifying the presence of TiO_2 in the respective TiO_2/GO compounds. The peak appearing at 461.3 eV corresponds to the Ti–C bond confirming the embedment of TiO_2 in the TiO_2/GO compounds via Ti–C linkage.

Fig. 5b presents the high-resolution spectrum of the C 1s peak fitted into four peaks. The main peak at 284.8 eV is attributed to sp^2-hybridized carbon (C–C) from the carbon layers. The peak at 286.1 eV originated from the hydroxyl carbon (C–O), and the peak at 288.7 eV is assigned to carboxyl carbon (O=C) or C–N. The Ti–C peak located at 283.9 eV demonstrates that part of the carbon was successfully embedded into the lattice of TiO_2 nanoparticles. Fig. 5c shows the O 1 s level spectra of the TiO_2/GO compounds. The O 1s signals can be deconvoluted into two peaks at approximately 530.8 and 532.1 eV. These peaks are attributed to the Ti–O and chemisorbed H_2O, respectively [49,50].

3.2. Microscopic characterization of the TiO_2/GO/PVDF composite membrane

3.2.1. Analysis of the chemical functional groups on the membrane surface

GO presented a typical FTIR spectrum with many distinct, strong absorption peaks corresponding to oxygen functional groups. As shown in Fig. 6b, a wide peak at approximately 3,422 and 1,360 cm^{-1} can be attributed to the OH and C–N stretching vibrations of GO. The GO curve shows a stretching vibration of CH at 3,178 cm^{-1}, and the four absorption peaks at 1,730; 1,620; 1,200 and 1,040 cm^{-1} are induced by the C–O, C=C, C–O, and C–O–C vibrations, respectively. Fig. 6a shows that the spectra of the PVDF-0, PVDF-1, PVDF-2, PVDF-3, and PVDF-4 membranes are essentially the same, and their vibration absorption peaks of C–OH, C–F, C–O–C, and C–H were found near 1,384; 1,186; 1,052 and 885 cm^{-1}, all of which came from PVDF.

The vibration absorption peaks of carbon = carbon double bonds (C=C) appear at 1,620 cm^{-1} in the PVDF-1, PVDF-2, PVDF-3, and PVDF-4 membranes. The vibration absorption peaks of hydroxyl (–OH) appear at 3,346 cm^{-1} in the PVDF-3 and PVDF-4 membranes corresponding to

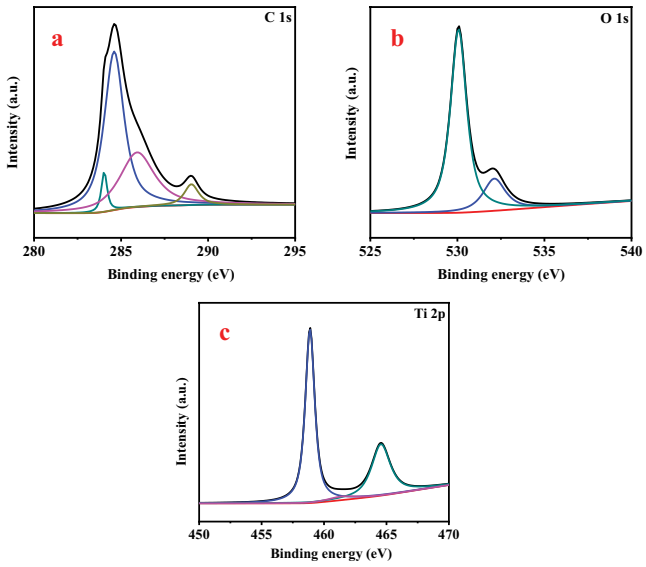

Fig. 5. X-ray photoelectron spectroscopy (XPS) of TiO_2/GO.

the tensile vibration of TiO_2/GO. The FTIR spectrum shows a new peak centered at 2,100 cm^{-1} in PVDF-3, which confirms the synergy of the TiO_2 and GO. Fig. 6a shows that the composite membrane did not change the structure of PVDF; TiO_2/GO was a physical combination. TiO_2/GO can introduce polar groups to improve the water flux and pollution resistance of a membrane [51]. The absorption peaks of –OH and C=C were stronger for the PVDF-3 membrane than for other membranes, indicating that the addition ratio was better.

3.2.2. Elemental characterization of TiO_2/GO/PVDF composite membrane

The crystal structures of the PVDF-0, PVDF-1, PVDF-2, PVDF-3, and PVDF-4 membranes were studied using XRD. As shown in Fig. 7, the characteristic peaks of the five membranes were almost the same. Characteristic peaks appear at 16.6°, 20.1°, and 23.2°, which is due to the PVDF. PVDF-2, PVDF-3, and PVDF-4 demonstrate weak peaks at 25.6° and 27.4°, deriving from the TiO_2/GO. Through careful observation, there are peaks at 29.2° for PVDF-2 and PVDF-3, peaks of PVDF-2 at 36.4°, and of PVDF-3 at 42.6°, which indicates the existence of TiO_2/GO. The reason why the characteristic peak is not strong is that the content of the TiO_2/GO composite is too small and the distribution of the TiO_2/GO on the surface of the PVDF membrane is relatively uniform.

3.2.3. Phase separation kinetics of the TiO_2/GO/PVDF composite membrane

Different membrane preparation conditions lead to different mass transfer processes, which affects the phase separation rate and membrane pore structure. By examining the change of absorbance of DMF in deionized water, the phase separation rate of the casting solution in the membrane forming process was analyzed. The absorbance of DMF in the casting solution of PVDF-0 was higher than PVDF-2 and PVDF-4, and lower than PVDF-1 and PVDF-3, which indicates that the addition of 1% and 5% TiO_2/GO particles increased the phase separation rate. This is because the barrier of nanoparticles reduces the interactions between the polymer and the solvent, making it easier for the solvent molecules to diffuse from the polymer matrix. In addition, PVDF-1 had the highest analysis rate.

The phase separation rate of PVDF membranes is related not only to hydrophilic particles but also to viscosity. As the amount of added particles increases, the viscosity of the prepared casting solution gradually increases (Fig. 8). The increase of viscosity is unfavorable to the diffusion of water and solvent and reduces the phase separation rate of the casting solution. It can be seen from the figure that, under the combined action of TiO_2/GO particles and the viscosity of casting solution, the phase separation rates of PVDF-1 and PVDF-3 were relatively high, which is conducive to the formation of the porous structure of the membrane, thus, improving the separation performance [51].

3.2.4. Thermodynamic properties of PVDF membranes

Fig. 9 shows that the pyrolysis process of the PVDF changed after adding TiO_2/GO. Clearly, the decomposition temperature of the PVDF-3 was higher than that of

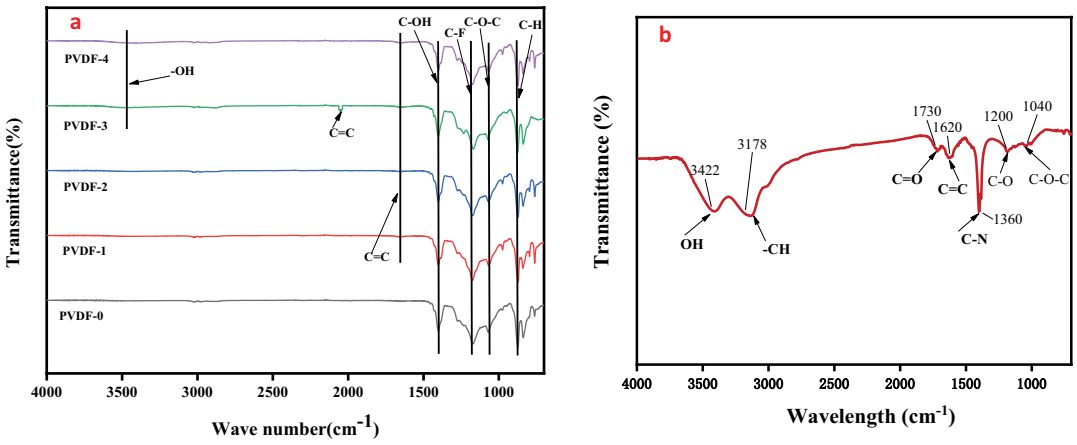

Fig. 6. Fourier-transform infrared (FTIR) spectra of (a) PVDF-0, PVDF-1, PVDF-2, PVDF-3, PVDF-4, and (b) GO.

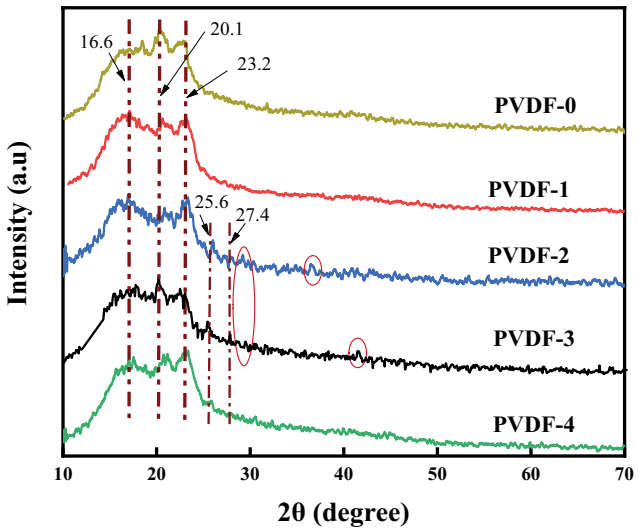

Fig. 7. XRD of PVDF-0, PVDF-1, PVDF-2, PVDF-3, and PVDF-4.

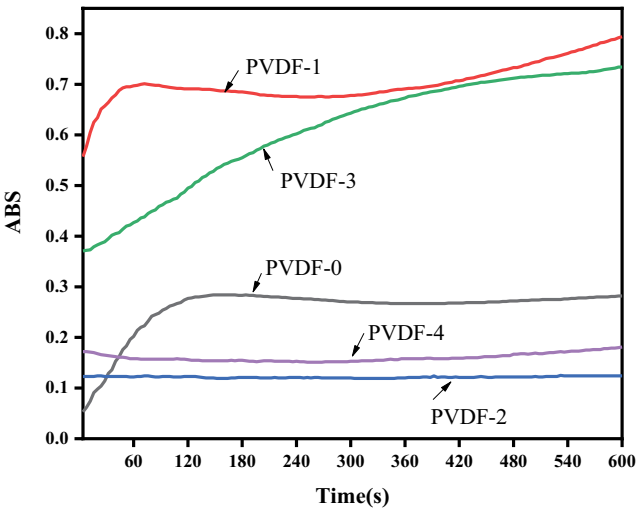

Fig. 8. The split-phase velocity of PVDF-0, PVDF-1, PVDF-2, PVDF-3, and PVDF-4.

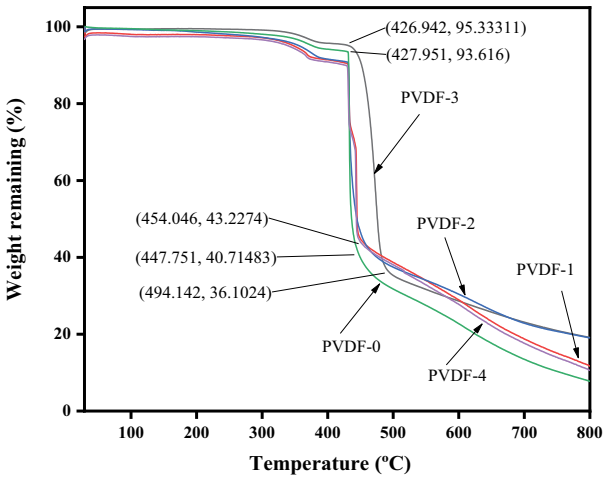

Fig. 9. Thermogravimetric analysis of PVDF-0, PVDF-1, PVDF-2, PVDF-3, and PVDF-4.

the other membranes. This phenomenon may indicate the decomposition of functional groups on the surface of the modified membrane. The results show that the added 3% TiO_2/GO became nucleation centers in the process of the PVDF solution-induced phase conversion, which affects the grain size and the void size of the PVDF formed in the process of membrane formation.

3.2.5. Morphology characterization of the membranes

As shown in Fig. 10, the difference of the microstructure on the surface of all membranes was not obvious, and they were all smooth. The cross-section is essentially a typical asymmetric structure composed of finger-like pores and sponge-like supporting layers, which shows that the basic morphology and structure of the membrane were not changed by adding particles. The number of pores at the bottom of the membrane increased and the distribution was more compact after adding TiO_2/GO, and the number of pores first increases and then decreases with the increase of the additive amount, which is consistent with the experimental results of the porosity measurements. The membrane cross-sectional spongy structure was reduced, the finger-like pores were increased and became more orderly, the pores first became larger and then tended to be stable, and they were connected from top to bottom, which is consistent with the experimental structure of the water flux measurement.

The change rules of the finger-like pores and porosity further prove that the phase separation rate first increased and then decreased with the increase of TiO_2/GO particles addition. The addition of fewer particles promoted the phase separation process, leading to the formation of larger finger-like pores. However, the addition of more particles led to a larger rate of the casting solution, thus, reducing the phase separation rate, leading to a reduction in the pore number and a small change in the pore size. This is consistent with the phase separation rate curve as measured by ultraviolet spectrophotometer.

3.3. Performance test of the composite membranes

3.3.1. Ultrafiltration performance of the composite membranes

As shown in Table 1, the porosity, water flux (J_w), BSA flux (J_p), and separation rate of PVDF-1, PVDF-2, PVDF-3, and PVDF-4 were higher than PVDF-0; however, the contact angle decreased, and the average pore diameter increased slightly. The results showed that the addition of particles increased the phase separation rate of the casting solution, changed the pores, increased the number of pores and the formation of macropores, and thus improved the hydrophilicity of the membrane. The ultrafiltration performance of PVDF-3 was the best, as the J_w was more than two times that of PVDF-0, the J_p increased from 35.6 L m^{-2} h^{-1} for PVDF-0 to 146.6 L m^{-2} h^{-1}, and the separation efficiency was also improved to about 91.2%.

Combined with Fig. 11, this shows that, after TiO_2 was modified by GO, more hydrophilic groups were

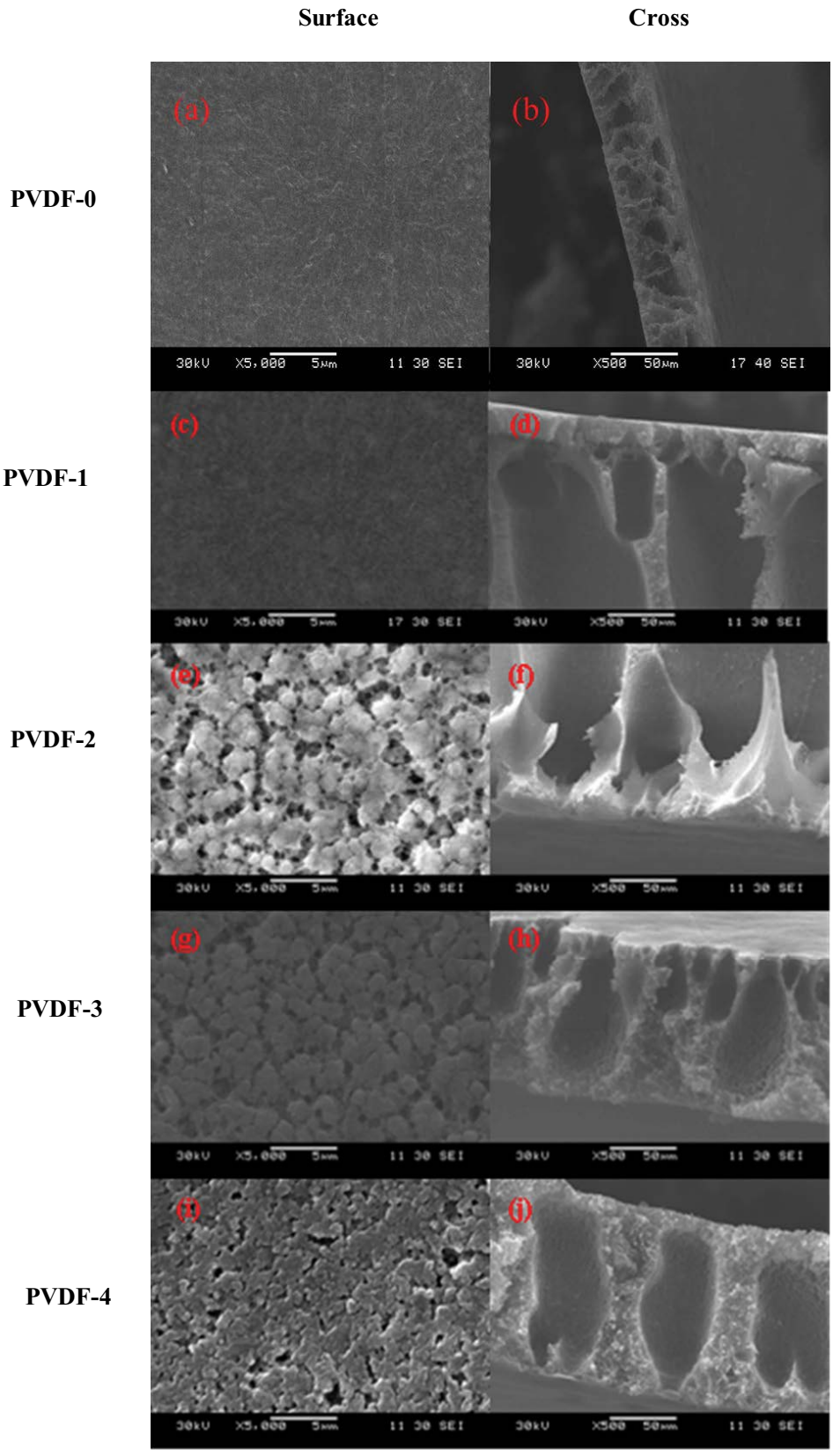

Fig. 10. SEM morphologies of PVDF-0, PVDF-1, PVDF-2, PVDF-3, and PVDF-4.

Table 1
Performance of the PVDF-0, PVDF-1, and PVDF-2 membranes

Membrane	ε	r_m	J_w	J_p	FRR	R	Contact angle
	(%)	(nm)	(L m^{-2} h^{-1})	(L m^{-2} h^{-1})	(%)	(%)	(°)
PVDF-0	50.6	38.02	90.3	35.6	68.03	64.7	87.6
PVDF-1	66.2	35.43	120.6	75.4	75.9	73.2	80.4
PVDF-2	67.8	39.11	170.5	98.4	86.8	80.3	73.2
PVDF-3	73.2	42.21	203.5	146.6	96.05	91.2	61.7
PVDF-4	68.8	42.67	186.8	124.6	91.17	85.3	70.8

FRR, flux recovery rate

introduced and a synergistic effect was produced to catalytically degrade part of BSA. All the BSA fluxes of the membranes were lower than the water flux, and the deionized water flushing produced restoration. Fig. 11 shows that the PVDF-3 flux recovery rate (FRR) was the highest, more than three times PVDF-0, which explains the improved stain resistance, mainly due to TiO_2/GO particles with more negative charges, PVDF-3, and the repulsive force between BSA enhancement, which has strong stain resistance.

3.3.2. Anti-fouling of the composite membranes

As shown in Fig. 12, the flux of PVDF-0 decreased significantly with the filtration time, while the PVDF-1, PVDF-2, PVDF-3, and PVDF-4 filtration curves showed a gentle downward trend. After 30% attenuation, this tended to be stable, and the required time increased from 180 min for PVDF-0 to 260, 310, 440, and 490 min, indicating that the filtration cycle and service life of the membrane after adding TiO_2/GO particles was significantly extended [46]. Notably, the downward trend of PVDF-3 was the least obvious, indicating the longest filtration cycle and service life.

The anti-fouling performance of the composite membrane was directly proportional to the FRR, and the stronger the anti-fouling performance was, the higher the FRR was (Fig. 13). The FRRs of the PVDF-0, PVDF-1, PVDF-2, PVDF-3, and PVDF-4 composite membranes were 68.03%, 75.9%, 86.8%, 96.05%, and 91.17%, respectively. The composite membranes were superior to PVDF-0 in pollution mitigation, and the hydrophilicity was also improved. In addition, the total pollution rates R_{FD} ($R_{FD} = R_{ir} + R_r$) of PVDF-1, PVDF-2, PVDF-3, and PVDF-4 were 49.3%, 30.85%, 27.97%, and 33.91%, which were lower than PVDF-0 (59.11%).

The corresponding reversible pollution and irreversible pollution were also reduced, because the stronger hydrophilic membrane more easily formed a hydration layer, reducing the contact between the membrane and the pollutant and, thus, enhancing the anti-fouling property of the membranes. The PVDF-3 composite membrane had the best anti-fouling performance, mainly due to the addition of the appropriate TiO_2/GO to carry a certain amount of negative charges, which increased the electrostatic repulsion against pollutants and reduced the membrane adsorption of pollutants.

4. Conclusion

The addition of TiO_2/GO particles prepared by the one-step synthesis method to the casting solution in different proportions, and the composite membrane prepared by phase transformation method demonstrated excellent hydrophilicity and anti-fouling properties. Compared with the PVDF-0 membrane, the specific results were as follows:

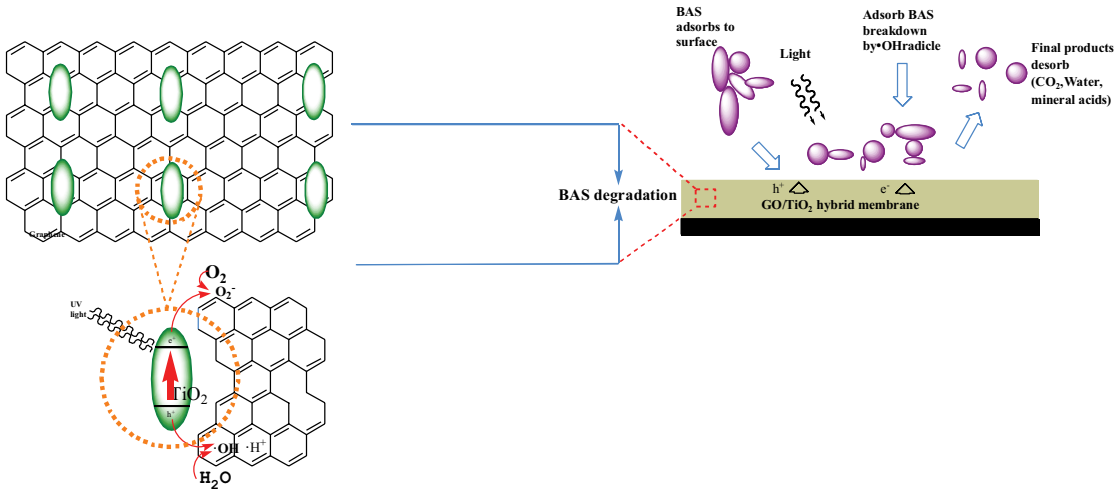

Fig. 11. Schematic of the membrane separation with bovine serum albumin (BSA).

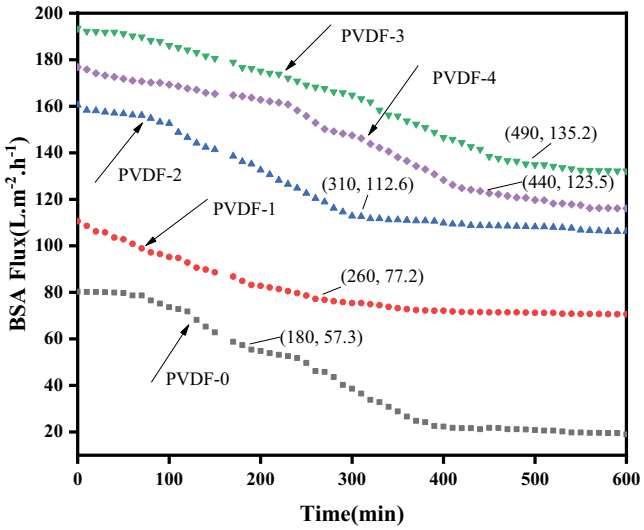

Fig. 12. The water flux varied with the filtration time in the interception process of BSA (0.1 g L^{-1}) for PVDF-0, PVDF-1, PVDF-2, PVDF-3, and PVDF-4.

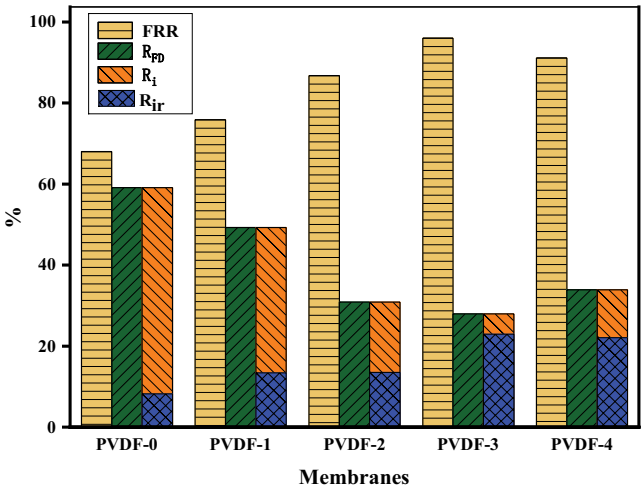

Fig. 13. Comparison of the FRR, R_{FD}, R_r, and R_{ir} of PVDF-0, PVDF-1, PVDF-2, PVDF-3, and PVDF-4.

- The TiO_2/GO particles were uniformly dispersed in groups in the casting solution without agglomeration. The separation, anti-fouling, and thermal properties were significantly improved.
- The PVDF-3 prepared with a TiO_2/GO addition ratio of 5% had a relatively large split phase velocity, the pores at the bottom were more abundant and evenly distributed, there were smoother and more ordered finger pores in the cross section and connected from top to bottom, and thus the PVDF-3 was highly hydrophilic and anti-fouling. The water flux and BSA flux were as high as 203.5 and 146.6 L m^{-2} h^{-1}, the FRR increased to 96.05% from 64.1% in PVDF-0, the contact angle decreased by 25.9°, and the total rate of pollution decreased from 59.11% in PVDF-0 to 27.97%. The downward trend of PVDF-3 was the least obvious from the results of the water flux variation with filtration time, indicating the longest filtration cycle and service life.

Conflicts of interest

The manuscript has not been published elsewhere and has not been submitted simultaneously for publication elsewhere. We also have no conflicts of interest to disclose. All authors have seen and approved the manuscript and have contributed significantly to the paper.

References

[1] C.Q. Zhao, J.L. Lv, X.C. Xu, G.Q. Zhang, Y.S. Yang, F.L. Yang, Highly antifouling and antibacterial performance of poly(vinylidene fluoride) ultrafiltration membranes blending with copper oxide and graphene oxide nanofillers for effrctive wasterwater treatment, J. Colloid Interface Sci., 505 (2017) 341–351.
[2] M.A. Shannon, P.W. Bohn, M. Elimelech, J.G. Georgiadis, B.J. Mariñas, A.M. Mayes, Science and technology for water purification in the coming decades, Nature, 452 (2008) 301–310.
[3] H. Guo, J.G. Bao, Q. Feng, J.K. Du, Y.F. Leng, Preparation of Ag_3PO_4/TiO_2-PVDF membrane and evaluation on antifouling properties, Environ. Sci. Technol., 41 (2018) 16–21.
[4] D. Rana, B.M. Mandal, S.N. Bhattacharyya, Miscibility and phase diagrams of poly(phenyl acrylate) and poly(styrene-*co*-acrylonitrile) blends, Polymer, 34 (1993) 1454–1459.
[5] D. Rana, B.M. Mandal, S.N. Bhattacharyya, Analogue calorimetric studies of blends of poly(vinyl ester)s and polyacrylates, Macromolecules, 29 (1996) 1579–1583.
[6] D. Rana, B.M. Mandal, S.N. Bhattacharyya, Analogue calorimetry of polymer blends: poly(styrene-*co*-acrylonitrile) and poly(phenyl acrylate) or poly(vinyl benzoate), Polymer, 37 (1996) 2439–2443.
[7] F. Liu, M.R. Moghareh Abed, K.Li, Preparation and characterization of poly(vinylidene fluoride) (PVDF) based ultrafiltration membranes using nano γ-Al_2O_3, J. Membr. Sci., 366 (2011) 97–103.
[8] F.M. Shi, Y.X. Ma, J. Ma, P. Wang, W.X. Sun, Preparation and characterization of PVDF/TiO_2 hybrid membranes with different dosage of nano-TiO_2, J. Membr. Sci., 389 (2012) 522–531.
[9] A. Rahimpour, M. Jahanshahi, B. Rajaeian, M. Rahimnejad, TiO_2 entrapped nano-composite PVDF/SPES membranes: preparation, characterization, antifouling and antibacterial properties, Desalination, 278 (2011) 343–353.
[10] J.-n. Shen, H.-m. Ruan, L.-g. Wu, C.-j. Gao, Preparation and characterization of PES–SiO_2 organic–inorganic composite ultrafiltration membrane for raw water pretreatment, Chem. Eng. J., 168 (2011) 1272–1278.
[11] C.J. Liao, J.Q. Zhao, P. Yu, H. Tong, Y.B. Luo, Synthesis and characterization of low content of different SiO_2 materials composite poly(vinylidene fluoride) ultrafiltration membranes, Desalination, 285 (2012) 117–122.
[12] L.-Y. Yu, Z.-L. Xu, H.-M. Shen, H. Yang, Preparation and characterization of PVDF–SiO_2 composite hollow fiber UF membrane by sol–gel method, J. Membr. Sci., 337 (2009) 257–265.
[13] X. Xie, J.G. Bao, S.H. Omer, H. Guo, Y. Zhou, H. Wang, Study for adsorption behaviors of emulsion oil on a novel ZrO_2/PVDF modified membrane, Desal. Water Treat., 57 (2016) 11736–11745.
[14] D.Y. Koseoglu-Imer, B. Kose, M. Altinbas, I. Koyuncu, The production of polysulfone (PS) membrane with silver nanoparticles (AgNP): physical properties, filtration performances, and biofouling resistances of membranes, J. Membr. Sci., 428 (2013) 620–628.
[15] M. Safarpour, S. Arefi-Oskoui, A. Khataee, A review on two-dimensional metal oxide and metal hydroxide nanosheets for modification of polymeric membranes, J. Ind. Eng. Chem., 82 (2020) 31–41.

[16] J.Z. Chen, X.R. Meng, Y.R. Tian, X.D. Wang, J.F. Zhu, H.Q. Zheng, L. Wang, Fabrication of a superhydrophilic PVDF-g-PAA@FeOOH ultrafiltration membrane with visible light photo-fenton self-cleaning performance, J. Membr. Sci., 616 (2020) 118587, doi: 10.1016/j.memsci.2020.118587.
[17] S. Anisah, M. Kanezashi, H. Nagasawa, T. Tsuru, Al_2O_3 nanofiltration membranes fabricated from nanofiber sols: preparation, characterization, and performance, J. Membr. Sci., 611 (2020) 118401, doi: 10.1016/j.memsci.2020.118401.
[18] J.Y. Zhu, S.Y. Zhou, M.S. Li, A.L. Xue, Y.J. Zhao, W.B. Peng, W.H. Xing, PVDF mixed matrix ultrafiltration membrane incorporated with deformed rebar-like Fe_3O_4–palygorskite nanocomposites to enhance strength and antifouling properties, J. Membr. Sci., 612 (2020) 118467, doi: 10.1016/j.memsci.2020.118467.
[19] J. Wang, Y.M. Wang, J.Y. Zhu, Y.T. Zhang, J.D. Liu, B. van der Bruggen, Construction of TiO_2@graphene oxide incorporated antifouling nanofiltration membrane with elevated filtration performance, J. Membr. Sci., 533 (2017) 279–288.
[20] C. Xu, A. Cui, Y.L. Xu, X.Z. Fu, Graphene oxide–TiO_2 composite filtration membranes and their potential application for water purification, Carbon, 62 (2013) 465–471.
[21] R.-X. Zhang, L. Braeken, P. Luis, X.-L. Wang, B. van der Bruggen, Novel binding procedure of TiO_2 nanoparticles to thin film composite membranes via self-polymerized polydopamine, J. Membr. Sci., 437 (2013) 179–188.
[22] M. Safarpour, V. Vatanpour, A. Khataee, Preparation and characterization of graphene oxide/TiO_2 blended PES nanofiltration membrane with improved antifouling and separation performance, Desalination, 393 (2016) 65–78.
[23] Y. Gao, M. Hu, B.X. Mi, Membrane surface modification with TiO_2–graphene oxide for enhanced photocatalytic performance, J. Membr. Sci., 455 (2014) 349–356.
[24] J.S. Li, Y. Liang, H.Y. Wang, X.Y. Sun, L.J. Wang, Preparation and characterization of TiO_2/PVDF composite hollow fiber membrane, Acta Polym. Sinica, 5 (2004) 709–712.
[25] E. Bet-Moushoul, Y. Mansourpanah, Kh. Farhadi, M. Tabatabaei, TiO_2 nanocomposite based polymeric membranes: a review on performance improvement for various applications in chemical engineering processes, Chem. Eng. J., 283 (2016) 29–46.
[26] H. Rabiee, M.H.D.A. Farahani, V. Vatanpour, Preparation and characterization of emulsion poly(vinyl chloride) (EPVC)/TiO_2 nanocomposite ultrafiltration membrane, J. Membr. Sci., 472 (2014) 185–193.
[27] S. Meng, J. Mansouri, Y. Ye, V. Vhen, Effect of templating agents on the properties and membrane distillation performance of TiO_2-coated PVDF membranes, J. Membr. Sci., 450 (2014) 48–59.
[28] Q. Zhou, J.-h. Li, B.-f. Yan, D. Wu, Q.-q. Zhang, Thermo-responsive and antifouling PVDF nanocomposited membranes based on PNIPAAm modified TiO_2 nanoparticles, Chin. J. Polym. Sci., 32 (2014) 892–908.
[29] J.-P. Méricq, J. Mendret, S. Brosillon, C. Faur, High performance PVDF-TiO_2 membranes for water treatment, Chem. Eng. Sci., 123 (2015) 283–291.
[30] Y.J. Zhao, F. Li, J.F. Li, C.Y. Ma, Comparison and analysis of PES ultrafiltration membranes modified by blending graphene oxide and nano-TiO_2, Membr. Sci. Technol., 36 (2016) 13–20.
[31] M. Safarpour, A. Khataee, V. Vatanpour, Effect of reduced graphene oxide/TiO_2 nanocomposite with different molar ratios on the performance of PVDF ultrafiltration membranes, Sep. Purif. Technol., 140 (2015) 32–42.
[32] Z. Arif, N.K. Sethy, L. Kumari, P.K. Mishra, B. Verma, Green synthesis of TiO_2 nanoparticles using *Cajanus cajan* extract and their use in controlling the fouling of ultrafiltration PVDF membranes, Korean J. Chem. Eng., 36 (2019) 1148–1156.
[33] N. Ma, Y.B. Zhang, X. Quan, X.F. Fan, H.M. Zhao, Performing a microfiltration integrated with photocatalysis using an Ag-TiO_2/HAP/Al_2O_3 composite membrane for water treatment: evaluating effectiveness for humic acid removal and anti-fouling properties, Water Res., 44 (2010) 6104–6114.
[34] S. Wang, The Coupling of FePc-TiO_2 with PVDF Membrane and the Treatment of Dye Wastewater, Dalian University of Technology, Dalian, 2016.
[35] G.K. Zhao, R.R. Hu, X.L. Zhao, Y.J. He, H.W. Zhu, High flux nanofiltration membranes prepared with a graphene oxide homo-structure, J. Membr. Sci., 585 (2019) 29–37.
[36] Y. Han, Z. Xu, C. Gao, Ultrathin grapheme nanofiltration membrane for water purification, Adv. Funct. Mater., 23 (2013) 3693–3700.
[37] R.K. Joshi, P. Carbone, F.C. Wang, V.G. Kravets, Y. Su, I.V. Grigorieva, H.A. Wu, A.K. Geim, R.R. Nair, Precise and ultrafast molecular sieving through graphene oxide membranes, Science, 343 (2014) 752–754.
[38] L. Yu, Y. Zhang, B. Zhang, J.D. Liu, H.Q. Zhang, C.H. Song, Preparation and characterization of HPEI-GO/PES ultrafiltration membrane with antifouling and antibacterial properties, J. Membr. Sci., 447 (2013) 452–462.
[39] M. Safarpour, A. Khataee, V. Vatanpour, Preparation of a novel polyvinylidene fluoride (PVDF) ultrafiltration membrane modified with reduced graphene oxide/titanium dioxide (TiO_2) nanocomposite with enhanced hydrophilicity and antifouling properties, Ind. Eng. Chem. Res., 53 (2014) 13370–13382.
[40] Y. Orooji, M. Faghih, A. Razmjou, J.W. Hou, P. Moazzam, N. Emami, M. Aghababaie, F. Nourisfa, V. Chen, W.Q. Jin, Nanostructured mesoporous carbon polyethersulfone composite ultrafiltration membrane with significantly low protein adsorption and bacterial adhesion, Carbon, 111 (2017) 689–704.
[41] Z.-w. Zhang, B. Xu, Y.-m. Zhang, F. Yang, M. Kong, Y.-m. Zhu, S.-y. Gu, X.-y. Guan, Removal of ammonia nitrogen from micro-polluted water by GO-TiO_2 modified PVDF composite membrane, China Environ. Sci., 39 (2019) 2395–2401.
[42] Z.W. Xu, T.F. Wu, J. Shi, K.Y. Teng, W. Wang, M.J. Ma, J. Li, X.M. Qian, C.Y. Li, J.T. Fan, Photocatalytic antifouling PVDF ultrafiltration membranes based on synergy of graphene oxide and TiO_2 for water treatment, J. Membr. Sci., 520 (2016) 281–293.
[43] M. Safarpour, V. Vatanpour, A. Khataee, M. Esmaeili, Development of a novel high flux and fouling-resistant thin film composite nanofiltration membrane by embedding reduced graphene oxide/TiO_2, Sep. Purif. Technol., 154 (2015) 96–107.
[44] L. Shao, S. Quan, Y. Liu, Z.H. Guo, Z.X. Wang, A novel "gel–sol" strategy to synthesize TiO_2 nanorod combining reduced graphene oxide composites, Mater. Lett., 107 (2013) 307–310.
[45] S. Ayyaru, T.T.L. Dinh, Y.-H. Ahn, Enhanced antifouling performance of PVDF ultrafiltration membrane by blending zinc oxide with support of graphene oxide nanoparticle, Chemosphere, 241 (2020) 125068, doi: 10.1016/j.chemosphere.2019.125068.
[46] D.M. Li, P. Jiang, T. Ye, S. Jiang, Study on preparation conditions and antifouling properties of GO-TiO_2 modified PVDF hollow fiber membrane, Acta Sci. Circum., 37 (2017) 3746–3754.
[47] L. He, J.G. Bao, Y.F. Leng, J.K. Du, K. Feng, A novel(H) g-C_3N_4/Ag_3PO_4/TiO_2 photocatalysis composite modified PVDF membrane and its evaluation on self-cleaning properties, Environ. Sci. Technol., 41 (2018) 26–33.
[48] V. Vaiano, O. Sacco, M. Matarangolo, Photocatalytic degradation of paracetamol under UV irradiation using TiO_2-graphite composites, Catal. Today, 315 (2018) 230–236.
[49] S.F. Shao, H.W. Kim, S.S. Kim, Y.Y. Chen, M. Lai, NGQDS modified nanoporous TiO_2/graphene foam nanocomposite for excellent sensing response to formaldehyde at high relative humidity, Appl. Surf. Sci., 516 (2020) 145932, doi: 10.1016/j.apsusc.2020.145932.
[50] L.F. Zhu, M.Y. Wu, B. Van der Bruggen, L.C. Lei, L.Z. Zhu, Effect of TiO_2 content on the properties of polysulfone nanofiltration membranes modified with a layer of TiO_2–graphene oxide, Sep. Purif. Technol., 242 (2020) 116770, doi: 10.1016/j.seppur.2020.116770.
[51] R.-Z. Pang, X. Li, J.-S. Li, Z.-Y. Lu, C. Huang, X.-Y. Sun, L.-J. Wang, In situ preparation and antifouling performance of ZrO_2/PVDF hybrid membrane, Acta Phys. Chim. Sin., 29 (2013) 2592–2598.